optica

High-dimensional quantum gates using full-field spatial modes of photons

Florian Brandt,[1,3] Markus Hiekkamäki,[2] Frédéric Bouchard,[3] Marcus Huber,[1] and Robert Fickler[1,2,*]

[1]Institute for Quantum Optics and Quantum Information (IQOQI), Austrian Academy of Sciences, Boltzmanngasse 3, A-1090 Vienna, Austria
[2]Photonics Laboratory, Physics Unit, Tampere University, Tampere, FI-33720, Finland
[3]Department of Physics, University of Ottawa, 25 Templeton Street, Ottawa, Ontario, K1N 6N5, Canada
*Corresponding author: robert.fickler@tuni.fi

Received 20 August 2019; revised 20 December 2019; accepted 20 December 2019 (Doc. ID 375875); published 23 January 2020

Unitary transformations are the fundamental building blocks of gates and operations in quantum information processing, allowing the complete manipulation of quantum systems in a coherent manner. In the case of photons, optical elements that can perform unitary transformations are readily available only for some degrees of freedom, e.g., wave plates for polarization. However, for high-dimensional states encoded in the transverse spatial modes of light, performing arbitrary unitary transformations remains a challenging task for both theoretical proposals and actual implementations. Following the idea of multi-plane light conversion, we show that it is possible to perform a broad variety of unitary operations at high quality by using only a few phase modulation planes. More importantly, we experimentally implement several high-dimensional quantum gates for up to five-dimensional states encoded in the full-field mode structure of photons. In particular, we realize cyclic and quantum Fourier transformations, known as Pauli $\hat{X}$-gates and Hadamard $\hat{H}$-gates, respectively, with an average visibility of more than 90%. In addition, we demonstrate near-perfect "unitarity" by means of quantum process tomography, unveiling a process purity of 99%. Last, we demonstrate the benefit of the two independent spatial degrees of freedom, i.e., azimuthal and radial, and implement a two-qubit controlled-NOT quantum operation on a single photon. Thus, our demonstrations open up new paths to implement high-dimensional quantum operations, which can be applied to various tasks in quantum communication, computation, and sensing schemes.

https://doi.org/10.1364/OPTICA.375875

1. INTRODUCTION

In times when optical quantum information processing tasks slowly enter the realm of everyday technical applications [1–4], reliable and efficient control of the Hilbert space of a quantum system becomes increasingly important. There are many optical elements known that perform unitary transformations [acting on different degrees of freedom (DOFs)] on certain input modes in order to achieve a desired mode content of the output. For instance, in polarization space, elements such as wave plates that make use of birefringence can be used to convert the photon's polarization states in a unitary fashion. The existence of such simple and efficient elements is one of the main reasons that this DOF has been used in a myriad of quantum experiments in both fundamental studies [2,5,6] as well as in applications [7,8]. However, it is known that high-dimensional systems, so-called *qudits*, offer access to several advantages such as an increase in channel capacity as well as an improved resistance to noise in communication protocols [9–11] with feasible experimental effort [12].

One very popular candidate for the implementation of high-dimensional information processing protocols that has gained a lot of attention in recent years is the transverse spatial DOF. A convenient and very popular discretization of two-dimensional transverse space can be done by using the Laguerre–Gauss (LG) modes [13,14], which form a complete, orthonormal basis. LG modes are characterized by a twisted helical wavefront of the form $e^{i\ell\phi}$, where ϕ is the azimuthal coordinate, and ℓ corresponds to the quantized orbital angular momentum (OAM) value [15], which can take on values as large as 10,010 [16]. In addition, LG modes are characterized by a second quantum number associated with the radial structure, which is often labeled p and has attracted notable attention only recently [17–20].

While there are infinitely many ways to decompose the continuous spatial DOF into orthogonal modes, LG modes with their OAM value are naturally conserved in down-conversion processes, which are the workhorse of experiments in photonic quantum information processing. This makes them a natural Schmidt basis

for analyzing entanglement and implementing quantum communication protocols. The family of LG modes has thus been the central matter of interest in various fields of experimental quantum information demonstrations using high-dimensional quantum states [21–27].

Here, the advances in technology to shape and detect the transverse structure of light with high precision has played a key role. In addition, the advantage of having multiple quantum states co-propagating along one optical axis, eases the implementation of more complex experimental arrangements due to intrinsic relative phase stability without the need for interferometric setups [28,29]. While the accessible Hilbert space is in principle infinite-dimensional, technical hurdles such as the aperture of the optical system or the resolution of cameras and tools for the manipulation of wavefronts limit the number of modes that can be harnessed in practical applications.

Nonetheless, experimental implementations already manage to access multiple modes with high fidelity. Indeed, for state generation, different optical techniques such as computer generated holograms [30,31] or direct modulation of the transverse phase [32,33] have been used. Measuring the spatial mode of single photons can also be considered a mature technology, with approaches ranging from mode sorting with the help of phase elements and free-space propagation [34–42] to mode filtering using phase- and intensity-flattening techniques along with single-mode-fiber coupling [21,43].

To truly harness the potential of this high-dimensional space, however, the ability to reversibly implement any transformation in the subspace spanned by a finite number of selected modes is crucial. And indeed, while the generation and measurement of transverse spatial modes have been investigated extensively, only a few unitary mode transformations have been realized despite their utmost importance for quantum information science. Early on, it was realized that cylindrical lenses arranged properly can transform a set of LG modes into Hermite–Gauss modes and vice versa [44]. More recently, a complex arrangement of bulk optical elements has been implemented to realize a universal gate on spin-orbit four-dimensional states [45], and a four-dimensional version of the $\hat{X}$-gate, i.e., a cyclic permutation of the input modes [46,47]. It has also been shown how to extend this to arbitrary dimensions using only linear optical elements arranged in complex interferometric setups and free-space propagation [48]. Thus, together with a mode-dependent phase operation (simply performed by a Dove prism), any unitary operation on the OAM subspace could be performed, at least theoretically.

A device that is able to perform any unitary operation within a given high-dimensional state space is often termed *multiport* and has been realized for path encoding [4,49] and similarly for the time–frequency domain [3,50]. For the transverse spatial DOF, only one experiment so far has demonstrated a single-mode conversion using multi-plane phase modulation implemented by a deformable mirror [51]. While the latter nicely demonstrates the potential of the technique, to the best of our knowledge, no experiment so far has demonstrated the implementation of a device that is able to perform any unitary operation between a set of input modes and a set of output modes of the full transverse spatial DOF of light.

Here, we present an experiment where we use a wavefront matching (WFM) technique [52,53] to implement a fully programmable multiport for transverse spatial modes of light in a multi-plane light-conversion (MPLC) setting. In contrast to earlier demonstrations of sorting, multiplexing, and beam steering [39,52,54,55], as well as single-mode conversions [51], we perform key quantum operations such as Pauli $\hat{X}$-gates and Hadamard $\hat{H}$-gates for multiple input and output modes taking into account both azimuthal and radial DOFs. We furthermore exploit the possibility of addressing all superposition states as inputs and outputs and perform full quantum process tomography. We find a process purity of 99% for cyclic transformations, which demonstrates the "unitarity" of the performed operation, a key measure for the quality of quantum information processing tasks. Finally, we perform a quantum operation on a single photon by taking advantage of the two "independent" transverse DOFs. In particular, we perform a controlled-NOT (CNOT) operation using both the radial and the azimuthal DOF of single photons, thereby highlighting the benefits of the ability to control the full-field structure of single quantum systems.

2. UNITARY TRANSFORMATIONS USING MPLC

The key task is to realize an experimental implementation of a so-called multiport that is able to perform any unitary operation $\hat{U}$ on a given set of d-dimensional input states ρ_i, i.e., in our case, a set of LG spatial modes, that converts them into a well-defined set of d-dimensional output states ρ_f:

$$\rho_f = \hat{U}\rho_i\hat{U}^\dagger. \tag{1}$$

The main idea behind our experimental realization of the unitary transformation $\hat{U}$ is that we use a multi-plane phase modulation technique to build a multiport, which shares similarities to some earlier work [51,52,54]. In this process, the device acts on all input modes at the same time; thus, no splitting of the modes or a separate phase-stable modulation is required. Instead of a stochastic optimization algorithm used earlier [51], we adapt the technique of WFM, which we outline below.

A. Wavefront Matching

The WFM technique is known from waveguide design [53] and has been used recently to perform LG mode sorting using multiple phase modulations [39]. During WFM optimization, all d input modes f_r are propagated forward through an optical system containing n phase elements Φ_t with some free-space propagation in between. At each modulation plane, $t = 1, \ldots, n$, the complex amplitudes of all modes $f_r(x, y, t)$ are recorded. Note that we do not perform a full Fourier transform between the phase modulations but use a split-step technique to propagate through the system. Subsequently, all final output or target modes b_s are propagated backwards, first to the last phase modulation plane ($t = n$) to obtain $b_s(x, y, n)$. Now all input–output mode pairs, i.e., f_r and b_s, where $r = s$, are "compared" to find the best single phase modulation that matches all wavefronts at the same time. For this, a field overlap between each input–output mode pair is calculated according to $o_{rst}(x, y) = \overline{b_s(x, y, t)}\, f_r(x, y, t)e^{i\Phi_t(x,y)}$, including a transverse phase modulation $\Phi_t(x, y)$, which is set to zero in the first iteration round but will be updated during the WFM process. Subsequently, the required phase patterns for the plane t can be obtained through

$$\Delta\Phi_t(x, y) = -\arg\left(\sum_{r=s} o_{rst}(x, y)e^{-i\phi_{rst}}\right), \quad (2)$$

where ϕ_{rst} is the average phase of the calculated overlap for each mode pair. The resulting phase modulation for the last plane $\Phi_n(x, y)$ is then imprinted on each backwards propagating mode b_s, which is then propagated to the $(n-1)$th modulation plane. Note that due to the free-space propagation between two phase modulations, the amplitude is slowly adjusted to match the input and output modes. At plane $(n-1)$, the overlaps between all input–output mode pairs are calculated again and the required phase change $\Delta\Phi_{n-1}(x, y)$ is obtained through the formula given in Eq. (2) and imprinted on all backwards propagating modes. Then, this procedure of propagating, comparing, and phase matching is repeated until the very first plane. During the subsequent propagation and modulation, the wavefronts of the backwards propagating modes approach the input modes with respect to their phase and amplitude until they are perfectly matching in the case of a very large number of phase elements n. If the number of phase modulations is limited, one iteration often leads to only a weak resemblance of the input–output mode pairs. However, the whole procedure can be repeated as many times as necessary until a certain fidelity is reached. We found that for all our calculations, we required only a maximum of 50 iterations, after which the mode overlaps between input and output modes did not improve anymore, while numerical errors slowly deteriorated the result. While the WFM technique has been used in different settings before [39,52,53], we use it as a powerful tool in our experiment to achieve the goals outlined above and presented below. As the input and output modes can be chosen freely, we now establish a procedure to implement any unitary operation between these modes, hence realizing a multiport using only a limited number of phase elements placed along the optical axis.

Before investigating how many phase elements are required to obtain reasonably good results, we briefly discuss a few important unitary operations that play a key role as important quantum gates in the field of quantum computation and quantum communication.

B. High-Dimensional Quantum Gates

Some of the most important unitary operations $\hat{U}$ in terms of high-dimensional quantum gates are the Pauli $\hat{X}$-gates, Hadamard $\hat{H}$-gates, as well as controlled-Pauli c$\hat{X}$-gates. The first two operations are single qudit operations and correspond to a cyclic transformation and a quantum Fourier transform, respectively. The third gate is a two-qudit operation, where one high-dimensional quantum system controls the cyclic operation on another high-dimensional quantum state. Note that for the latter, the two-qubit version is also known as a controlled-NOT operation.

1. $\hat{X}$-Gate

The effect of a high-dimensional $\hat{X}$-gate (i.e., cyclic transformation) on a certain d-dimensional quantum state can be mathematically expressed as

$$\hat{X}^m|l\rangle = |(l+m)_{\mathrm{mod}(d)}\rangle, \quad (3)$$

which simply corresponds to a cyclic operation where each mode gets transformed to its m-th nearest-neighbor mode, modulo the number of modes d. Interestingly, it was shown only recently and only for the OAM DOF that this operation can be implemented for arbitrary dimensions using a complex arrangement of linear optical elements and free-space propagation [48]. For full-field modes, i.e., including both azimuthal and radial modes, no implementation of cyclic transformations is known. Examples of matrix representations of these gates for dimension three, i.e., qutrits, can be found in Supplement 1.

2. Hadamard Gate

The high-dimensional quantum Fourier transform operation is also known as a high-dimensional Hadamard $\hat{H}$-gate due to its relation to the well-known Hadamard gate for qubits. Its mathematical representation for prime dimensions (larger than two) can be formulated as

$$\hat{H}_m|\Psi_l\rangle = \frac{1}{\sqrt{d}}\sum_{k=0}^{d-1}\omega_d^{(lk+(m-1)k^2)}|k\rangle, \quad (4)$$

where $\omega_d = e^{i2\pi/d}$, $m = 1, \ldots, d$, and $\hat{H}_0$ is the identity. This operation transforms any given input state of a basis into a coherent superposition of all the modes of that basis with different well-defined phases. The different configurations of the Hadamard gate $\hat{H}_m$ can be seen as a simple change between mutually unbiased bases (MUBs). While the switching among all possible MUBs is important for various quantum tasks, e.g., for quantum state tomography and cryptography [56], there is one basis that is intuitively simple to understand for LG modes with $p = 0$ and OAM values symmetrically distributed around $l = 0$, because it corresponds to a transformation into angular coordinates. Again, we note that there is no bulk optics realizations known for such operations. For the four different Hadamard transformation matrices for qutrits, we refer to Supplement 1.

3. Controlled $\hat{X}$-Gate

The final quantum operation we discuss here and implement in our experiment below is a gate requiring two high-dimensional quantum states, where one is used to control the other, i.e., a controlled-$\hat{X}$-gate or c$\hat{X}$-gate. Its mathematical representation can be formulated as follows:

$$c\hat{X}(|p\rangle|l\rangle) = (\hat{I}\otimes\hat{X}^p)|p\rangle|l\rangle = |p\rangle|(l+p)_{\mathrm{mod}(d)}\rangle. \quad (5)$$

The commonly known qubit version is the so-called CNOT gate, where one qubit acts as a control qubit for a second target qubit, on which a NOT operation is performed if and only if the control qubit is $|1\rangle$ and leaves it unchanged if it is $|0\rangle$. Generalized to arbitrary dimensions for both the control and target qudits, the operation acts as a cyclic operation on the target qudit, where the state is shifted by the value of the control qudit. In our case, one qudit, e.g., the control qudit, can be realized by the radial DOF of light, while the target qudit corresponds to the OAM value. Thus, if the input photon has a radial structure of p, the OAM value l is shifted by p modulo the dimension of l. In Supplement 1, we give the transformation matrix of a two-dimensional CNOT gate as an example.

C. Implementation Using MPLC

We now turn to the investigation of how many planes are required to realize the above-discussed d-dimensional quantum gates using multi-plane phase conversion. First, we calculate the phase modulations using two, three, five, and eight phase elements for two, three, four, five, seven, and 11 OAM modes for the $\hat{X}^1$-gates and $\hat{H}_d$-gates using the WFM method. As an example of one simulated unitary operation, we show the scheme of a qutrit $\hat{X}^1$-gate for the LG modes with $p = 0$ and $l = 0, \pm 1$ using three planes of phase modulation in Fig. 1(a). Similar to Refs. [51,52], we find that if the number of modes exceeds the number of planes, the quality of the transformation decreases significantly. As a measure of the quality of the transformation, we use the *visibility* V, which we obtain from the crosstalk measurements between the input and output modes in one basis, i.e., the initially defined computational basis, according to

$$V = \sum_i C_{ii} / \sum_{ij} C_{ij}, \tag{6}$$

where C_{ij} corresponds to the probability entries in the diagonal crosstalk matrix, and C_{ii} signifies the probability of the input mode being transformed into the desired output mode. We observe very low crosstalk, i.e., a visibility V in excess of 96%, when the number of modes is equal to the number of planes and only up to five modes are used [see Fig. 1(b)]. Since simple crosstalk matrices measured in one basis cannot directly reveal information about the unitarity of the mode transformation, we also perform a full high-dimensional quantum process tomography [57] on the simulated three-dimensional $\hat{X}^1$-gate.

Quantum process tomography is based on a set of informationally complete measurements for a given set of input states, leading to a complete characterization of the corresponding quantum channel. The channel can then be represented by a completely positive map $\mathcal{E}$, where $\rho_f = \mathcal{E}(\rho_i)$. Using a fixed set of operators, $\mathcal{E}$ can be expressed as

$$\mathcal{E}(\rho) = \sum_{i,j} \chi_{i,j} \hat{\sigma}_i \rho \hat{\sigma}_j^\dagger, \tag{7}$$

where χ is a $d^2 \times d^2$ dimensional matrix known as the process matrix, and $\hat{\sigma}$ are the Gell–Mann matrices, also known as Pauli matrices for $d = 2$. Hence, this representation of quantum processes can describe more general processes, e.g., decoherence of the input state, than for the case of unitary transformations ($\mathrm{rank}(\chi) = 1$). Note that besides our approach of quantum process tomography for the complete characterization of the system (transformation), various equally valid classical analogs can be used to obtain the complex transformation matrix [58]. The unitarity of the transformation can be assessed by taking advantage of the Choi–Jamiolokowski isomorphism, which implies that $\mathcal{E}$ can be represented by an operator $\rho_{\mathcal{E}}$, known as the Choi matrix, given by

$$\rho_{\mathcal{E}} = \left(\hat{I} \otimes \mathcal{E}\right) |\Psi\rangle\langle\Psi|, \tag{8}$$

where $|\Psi\rangle$ is a d-dimensional maximally entangled state. Thus, the *process purity*, $\mathrm{Tr}[\rho_{\mathcal{E}}^2]$, is a measure of the extent to which the purity of the input states is maintained throughout the quantum process [59]. As expected, we find almost perfect process purity in simulation, irrespective of the number of phase elements [see Fig. 1(b)]. In order to perform process tomography, we propagate all states of all MUBs through the device and compare the simulated outcome with the targeted modes to obtain a correlation matrix. From this matrix, one can also deduce key figures of merit, such as the *transformation efficiency*, which is a measure of how much light remains within the utilized subset of modes. Again, we find that already three planes are sufficient to get very good results of more than 80% transformation efficiency for three modes [see Fig. 1(b)].

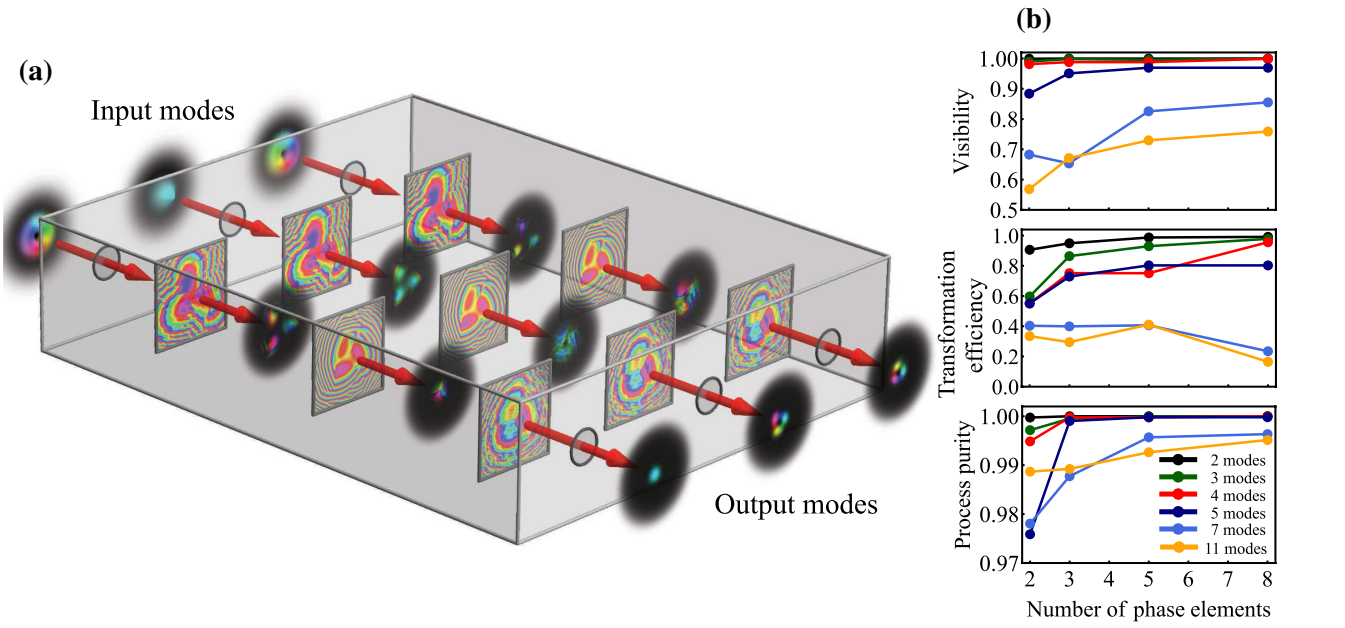

Fig. 1. Presentation of the multi-plane light-conversion (MPLC) technique. (a) Simulated evolution of the input modes at different stages of the MPLC setup is shown for the case of three phase elements. We note that the input modes are all co-propagating and therefore experience the same three phase manipulations. (b) Simulated visibility, transformation efficiency, and process purity of the cyclic transformation are shown as a function of the number of phase elements for different numbers of OAM modes.

Having shown that only a few phase planes are enough to enable a broad range of quantum gates in simulations, we now implement a simple experimental realization of a quantum gate.

3. EXPERIMENTAL RESULTS

A. X-Gate Using Three Phase Modulations and OAM Qutrits

As a first experimental test and benchmark of a multiport realized by MPLC, we implement the three-dimensional $\hat{X}^1$-gate for LG modes $\{|l=-1\rangle, |l=0\rangle, |l=1\rangle\}$ and $p=0$ by using only three modulation planes. We start with a low number of modes and phase modulations to investigate a best-possible implementation in terms of efficiency, resolution, and modulation ability. We further use only LG modes with no radial structure to minimize errors introduced by the detection system [43]. A sketch of the experimental setup can be seen in Fig. 2(a). At first, we imprint the required LG mode structures on a spatially cleaned 808 nm laser beam with a strongly enlarged Gaussian mode and carve out the required LG mode by modulating the phase and amplitude of the light using a single spatial light modulator (SLM-A) [60]. We then implement the multiport by another SLM (SLM-B) in combination with a mirror opposing it. The laser is sent through this arrangement such that it bounces off the SLM three times, which enables three separate phase modulations. Each of the three phase modulations covers a large area of 630×630 pixels on the SLM to reduce errors introduced by the finite resolution of the holograms. We further reduce errors introduced by slight (pixel-sized) misalignments by using a beam waist of around 1 mm, which is much larger than the pixel pitch (8 μm). The propagation distance between each phase modulation, i.e., each reflection on the SLM, is set to 800 mm, thus ensuring sufficient propagation for phase-induced amplitude modulation and a proper functioning of the mode conversion. The utilized phase modulations are the ones presented in Fig. 1. We note that in our experiment, we additionally imprint a diffraction grating and use only the first diffraction order, thereby filtering out the unmodulated light remaining in the zeroth order. We additionally decrease the beam waist of the modes during the transformation by a factor of two (implemented by the WFM code), to have a smaller beam impinging on the third SLM (SLM-C) in order to improve the measurement, which uses phase and intensity flattening of the beam to ensure, although lossy, near-perfect spatial mode projections [43]. With this configuration, we achieve a three-dimensional X^1-gate with a visibility V of $(98.4 \pm 0.7)\%$ between all 144 input–output mode combinations of all four MUBs [see full crosstalk matrix in Fig. 2(c)]. This result is close to the one expected from simulation of 99.6% [Fig. 2(b)] and shows the near-perfect functioning of the experimental implementation of our multiport. Furthermore, we perform high-dimensional quantum process tomography of the experimental three-dimensional $\hat{X}^1$-gate, for which the theoretical process matrix can be seen in Figs. 3(a) and 3(b). The experimentally reconstructed process matrix is shown in Figs. 3(c)–3(d). We find a process purity of 99.3%, which is in perfect agreement with the simulated prediction. Moreover, the process purity shows nicely that the transformation is fully coherent and as such, a powerful tool in quantum information schemes.

B. High-Dimensional Gates for OAM Modes

As we have shown earlier, a larger number of phase modulations allows unitary operations on a larger mode set and as such, a larger dimension of the quantum state. To test the limitations in terms of simplicity of the experimental implementation and maximum number of phase modulations, we now realize a setup with a multiport consisting of eight phase modulations, as well as the generation and detection on the same SLM screen, i.e., a setup where the beam bounces off the SLM 10 times in total. In contrast to the experimental setup shown in Fig. 2(a), we now implement

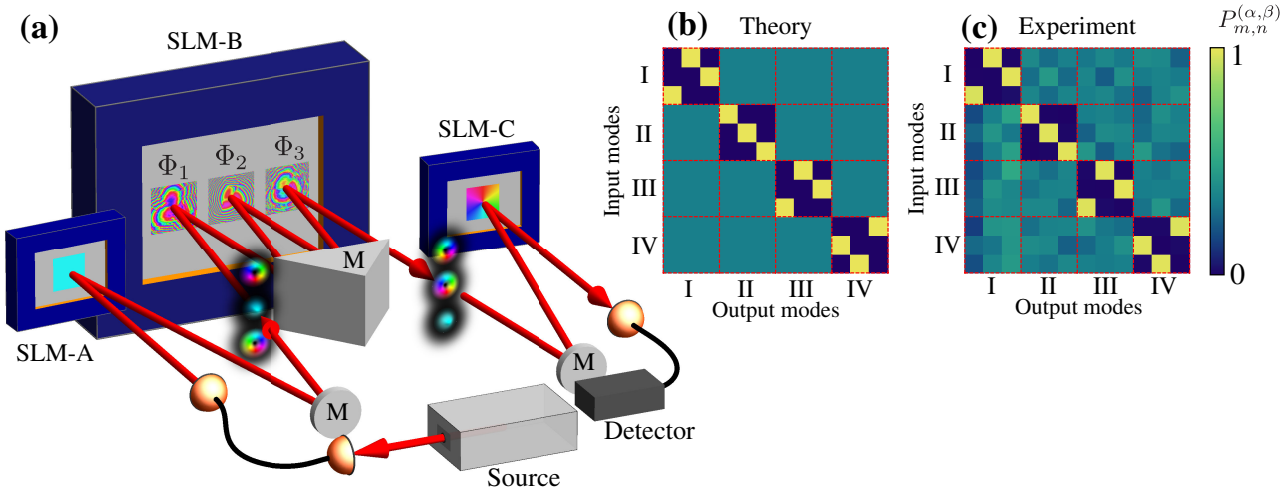

Fig. 2. Experimental implementation of the three-dimensional cyclic transformation. (a) Simplified experimental setup showing the implementation of the three-dimensional $\hat{X}$-gate using three phase elements. Photons from the source are spatially filtered to the fundamental Gaussian mode using a single-mode fiber (black wire). The beam is then made incident on SLM-A, where both the phase and amplitude are manipulated in order to generate the appropriate LG mode. These modes are then fed into the MPLC system consisting of SLM-B, displaying three phase patterns, and a mirror (M). The beam bounces off between the SLM and the mirror three times before it exits the system and is detected using SLM-C with the intensity-flattening technique introduced only recently in Ref. [43]. (b) Theoretical prediction of a tomographically complete set of measurements for the theoretical three-dimensional $\hat{X}$-gate. The input and output states are chosen from the three-dimensional MUBs labeled here by I, II, III, and IV. (c) Experimental correlation matrix for different MUBs obtained from the MPLC system described in (a).

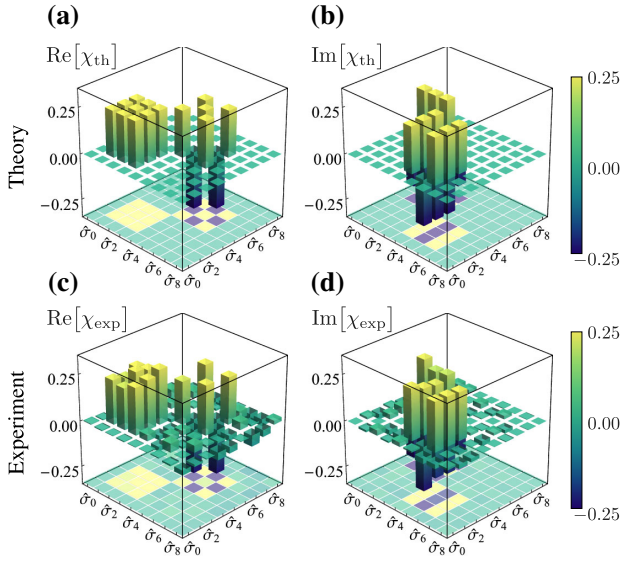

Fig. 3. Quantum process tomography of the three-dimensional cyclic transformation. The real (a) and imaginary (b) parts of the theoretical process matrix, χ_{th}, for the three-dimensional $\hat{X}$-gate are shown in the Gell–Mann matrix basis. The real (c) and imaginary (d) parts of the experimentally reconstructed process matrix, χ_{exp}, for the experimental implementation of the three-dimensional $\hat{X}$-gate using three phase elements and OAM modes $\ell = -1, 0, 1$ are shown in the Gell–Mann matrix basis.

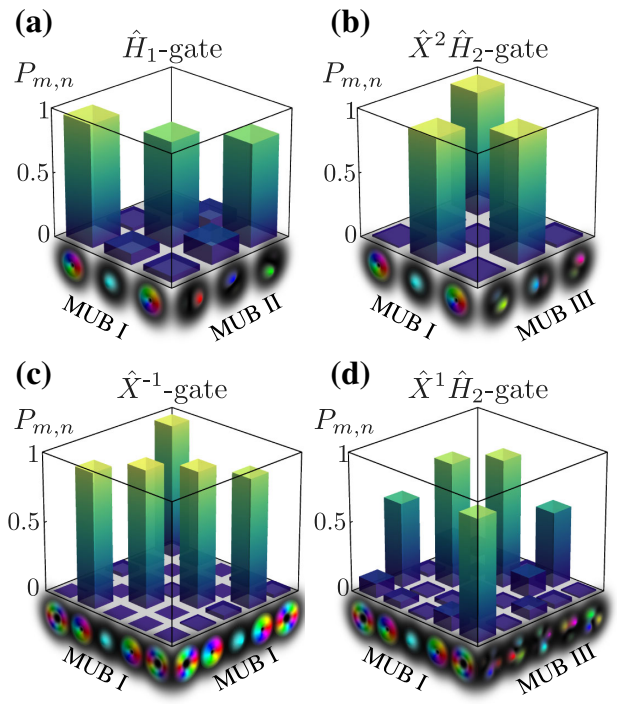

Fig. 4. Experimental results for the OAM transformations using a single SLM for generation, manipulation (eight phase planes), and detection. Crosstalk matrices are shown for a three-dimensional Hadamard gate ($\hat{H}_1$), converting input beams from the computational basis to another mutually unbiased basis (here, the angle basis) (a) and a Pauli $\hat{X}^1$-gate in dimension five (c). We further realize combined $\hat{X}\hat{H}$ operations performing a cyclic operation on a set of input modes that is transformed to another MUB in dimension three ($\hat{X}^2\hat{H}_2$-gate) (b) and dimension five ($\hat{X}^1\hat{H}_2$-gate) (d). Note that the quality for measurements of complex superposition modes in large Hilbert spaces as in (d) decreases due to limited resolution of the holograms for the single-SLM implementation.

five reflections on the upper half of the SLM, each phase modulation being 160 × 160 pixels in size. Here, we use a beam of around 0.5 mm waist, and we propagate it only 100 mm between each phase modulation (50 mm between mirror and SLM), to keep the whole setup more compact. After the fifth reflection, we insert another slightly tilted mirror into the setup, which sends the light back onto the lower part of the SLM, where the beam bounces off the SLM another five times before it can leave the MPLC arrangement. Since we have to redirect the light from the upper to the lower half of the SLM, we compensate this vertical redirection of the beam by displaying additional horizontal grating structures on the five holograms displayed on the lower half of the SLM. For the generation (done by the first hologram) and the detection of the modes (last hologram), we again use amplitude and phase modulation [60] as well as phase and intensity flattening [43]. As there are now 10 relatively small holograms in total, a misalignment of only one pixel for each hologram leads to a significant reduction in the quality of the mode transformation. Moreover, when a larger number of modes is involved, the phase modulations calculated by the WFM tend to get more complicated, which makes the alignment even harder. Due to this fact, we make use of an automated alignment procedure based on a genetic algorithm [61], where each member of the population defines the positions of all holograms, and the feedback signal is given by the visibility V of the crosstalk measurements of the transformation as defined in Eq. (6). With this programmable and fully automated multiport, we are now able to test various transformations and single-qudit gates for different modes and dimensions.

In a first set of measurements, we use only LG modes with radial index $p = 0$. For a three-dimensional state space spanned by the three lowest OAM modes, i.e., the set $\{|l = -1\rangle, |l = 0\rangle, |l = 1\rangle\}$, we experimentally obtain an average visibility of $(92.7 \pm 3.8)\%$ for all three possible $\hat{X}$-gates in the computational basis (MUB I). We further measure an average visibility of $(92.0 \pm 3.0)\%$ for basis-change transformations, i.e., a Hadamard $\hat{H}$-gate, followed by a cyclic operation of the states in the new basis, i.e., a Pauli $\hat{X}$-gate, which corresponds to the unitary transformation $\hat{U} = \hat{X}\hat{H}$. The exact results of all recorded correlation matrices for this as well as for all following measurements can be found in Supplement 1.

We then increased the dimension to $d = 5$ by including second-order OAM modes, i.e., $|l = -2\rangle$ and $|l = 2\rangle$. We obtained an average visibility over all $\hat{X}$-gates in the computational basis of $(91.9 \pm 3.2)\%$. However, for the modes of the other MUBs, the obtained visibility of the crosstalk matrix does not reach the theoretical value but is found to be only 76.5% [see Fig. 4(d)]. We relate this decrease in transformation quality to the finite resolution of our SLM, i.e., to be of only technical nature, the reason being that the complexity of the spatial structure of higher-order superposition modes (the states of the other MUBs), i.e., the field gradients, is comparable in size to the pixels of the SLM. This means that a misalignment of one pixel already has a significant effect on the quality of the transformation. In contrast, if the phase gradient is smooth and small—as is the case for states in the computational basis—slight misalignments do not have a big effect. Examples of several recorded correlation matrices for different OAM transformations can be seen in Fig. 4.

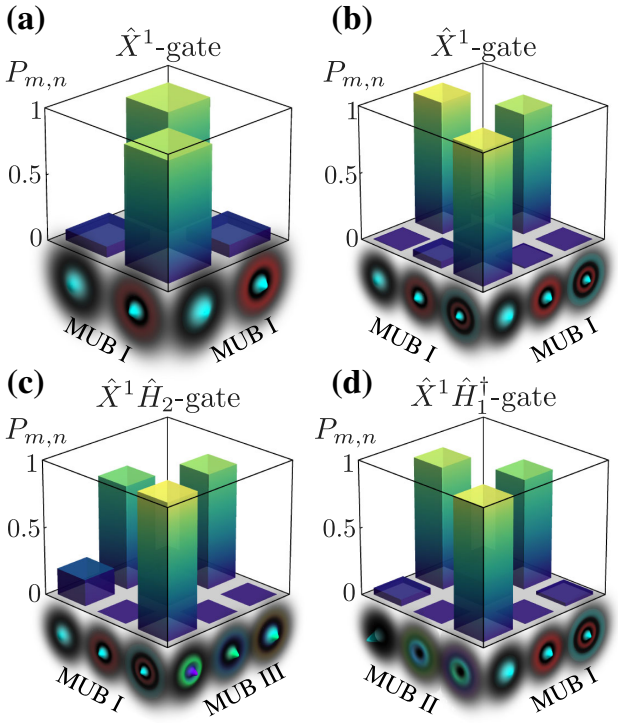

Fig. 5. Experimental results of different p-mode transformations, again using only one SLM for generation, manipulation, and detection. A cyclic transformation $\hat{X}^1$ on p-only modes in the computational basis is shown for dimension two in (a) and dimension three in (b). In addition, we implement also combined $\hat{X}\hat{H}$-gates in dimension three, in particular, a $\hat{X}^1\hat{H}_2$-gate shown in (c) and a $\hat{X}^1\hat{H}_1^\dagger$-gate shown in (d). Note that measuring p-modes properly in different mutually unbiased bases has become possible only recently [43].

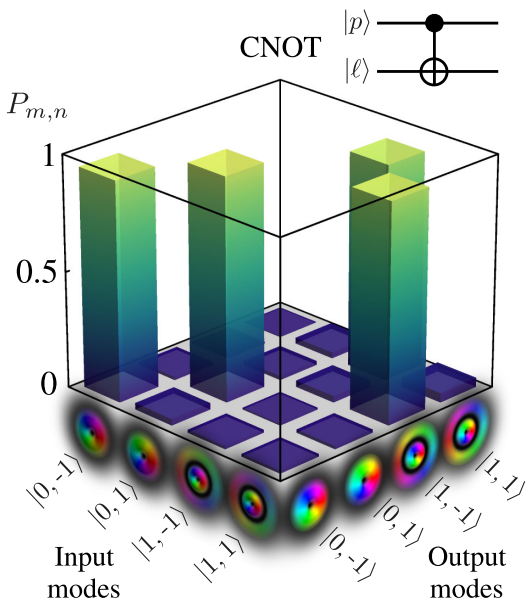

Fig. 6. Single-photon CNOT gate using the radial modes $|p\rangle$ as a control qubit for the manipulation of the azimuthal modes $|\ell\rangle$. Experimental crosstalk matrix with input and output modes labeled by the states $|p, \ell\rangle$. A visibility of 94.6% is achieved for the single-photon CNOT gate with a MPLC system consisting of a generation SLM, an SLM used for the manipulation (consisting of three phase planes), and one SLM as the detection SLM. The quantum circuit diagram of a CNOT gate as used frequently in quantum information science is also shown in the top right corner.

C. High-Dimensional Gates for Radial Modes

While the OAM transformations performed above can be (at least in theory) realized using bulk optical elements [48], we now turn to mode transformations of radial modes, i.e., p-modes, a task for which no other implementation is known so far and therefore represents another novelty of our work. In particular, this experimental demonstration is now possible due to the recently developed measurement technique, known as intensity flattening [43], which enables the detection of p-modes in all MUBs and thus makes it possible to measure perfectly the full-field structure of LG beams with only a minor experimental trade-off, i.e., additional loss. We performed $\hat{X}$-gates in the p-only space of LG beams ($l = 0$) for qubits and qutrits using the set $\{|p = 0\rangle, |p = 1\rangle\}$ and $\{|p = 0\rangle, |p = 1\rangle, |p = 2\rangle\}$, respectively. Additionally, we performed $\hat{H}$-gates and combined $\hat{X}\hat{H}$-gates for the same mode set (see Fig. 5 for examples). The average visibility obtained over all transformations performed is $(92.4 \pm 3.4)\%$, which shows nicely that our experimentally implemented multiport is able to perform not only OAM transformations but also operations on full-field modes, including both azimuthal and radial DOFs, an advantage that we harness in the following section.

D. Single-Photon Controlled-X Gate

As a final test, we perform the controlled-$\hat{X}$ operation, i.e., the c$\hat{X}$-gate, introduced earlier. In contrast to the usual implementation using two quantum systems, we use two spatial DOFs of a single quantum system. In order to perform this task on an actual quantum system, we exchange the laser with a heralded single-photon source. The single photons are generated by a photon pair source realized by a type II parametric down-conversion process (periodically poled potassium titanyl phosphate nonlinear crystal) pumped by a 405 nm laser source. One of the two photons acts as a trigger signal to herald the existence of the single photon on which the quantum operation is performed.

In our demonstration, we perform the two-dimensional version of this gate, which is one of the most important quantum operations, i.e., the CNOT gate. The control qubit is encoded in the radial structure of the photon $\{|p = 0\rangle, |p = 1\rangle\}$, while the target qubit corresponds to the OAM quantum number $\{|l = -1\rangle, |l = 1\rangle\}$. To put it into simple terms: the CNOT operation performs a cyclic transformation on the OAM value, depending on the radial quantum number. For efficiency reasons, we realize this single-photon quantum gate with the first configuration of the multiport, i.e., using only three phase modulations on the manipulation SLM (SLM-B) and performing the generation and detection on two additional, separate SLMs (SLM-A and SLM-C). According to simulations, three phase modulation planes already allow a visibility of 96% and, more importantly, increase the efficiency approximately by a factor of five due to a reduced number of reflections on the SLM. The resulting correlation matrix is shown in Fig. 6, which corresponds to a visibility of $(94.7 \pm 1.4)\%$, which is very close to the theoretical prediction.

4. CONCLUSION AND OUTLOOK

In conclusion, we have proposed and experimentally demonstrated an easy to implement, versatile scheme that can perform in principle arbitrary unitary transformations on spatial modes of light. Our method has the advantage of being simple and straightforward to implement, therefore making it a novel experimental tool for future experiments, especially in the field of quantum information processing. In order to demonstrate the versatility of our technique, we demonstrated applications of different quantum gates on three- and five-dimensional LG modes, taking into account both the radial as well as the azimuthal quantum number. Besides the conventional high-dimensional versions of the Pauli $\hat{X}$-gate and the Hadamard $\hat{H}$-gate, as well as combinations thereof, we also implemented a single-photon CNOT gate, harnessing one transverse coordinate to control the other one. Moreover, we performed quantum process tomography on one particular transformation, unveiling the "unitarity" of the operation. While the demonstrated $\hat{X}$- and $\hat{H}$-gates are fundamental building blocks for high-dimensional quantum information processing tasks, Hadamard $\hat{H}$-gates can also be highly valuable as a switch between different MUBs in quantum cryptography applications. Moreover, the CNOT gate performed on a single photon, demonstrates nicely additional opportunities offered by having access to the two independent DOFs when using transverse spatial structures such as high-dimensional quantum states. We hope that this might trigger research in less explored avenues of quantum information processing, e.g., in simplifying quantum gates [62].

A central challenge that will have to be addressed in the future is the limited single-photon efficiency, due to losses incurred by every reflection upon the SLM, in our case, a loss of around 25%. For fixed quantum information protocols (e.g., quantum key distribution, where only a few bases, fixed by the protocol are required) or fundamental tests, this downside can be overcome by physically designing phase plates corresponding to the individual phase modulations, e.g., as has been shown in multiplexing tasks [54]. This would lead to high-fidelity and low-loss arbitrary unitary transformations, but would sacrifice the flexibility to program any transformation and requires a pre-designed piece of equipment for every basis. A solution that is still flexible and can be used as a re-programmable multiport can be the implementation using deformable mirrors. They usually have very high reflection efficiencies, however, can become very costly when high spatial resolutions of the modulation are required. Nevertheless, our implementation adds another important tool for high-dimensional quantum information experiments using spatial modes of light and shows the potential that this set of modes offers, especially if both radial and azimuthal DOFs are taken into account.

Funding. Austrian Science Fund (Y879-N27); Czech-Austrian project MultiQUEST (GF17- 33780L, I 3053-N27); Natural Sciences and Engineering Research Council of Canada (Vanier Canada Graduate Scholarships Program); Academy of Finland (301820, 320165).

Acknowledgment. We thank A. Zeilinger and E. Karimi for many fruitful discussions. FBr, RF, and MHu acknowledge funding from the Austrian Science Fund (FWF) through the START and the joint Czech-Austrian project MultiQUEST. FBo acknowledges the support of the Vanier Canada Graduate Scholarships Program and the Natural Sciences and Engineering Research Council of Canada (NSERC) Canada Graduate Scholarships program. RF and MHi acknowledge the support of the Academy of Finland through the Competitive Funding to Strengthen University Research Profiles and the Photonics Research and Innovation Flagship.

Disclosures. The authors declare no conflicts of interest.

See Supplement 1 for supporting content.

REFERENCES

1. J. P. Dowling and G. J. Milburn, "Quantum technology: the second quantum revolution," Philos. Trans. R. Soc. London, Ser. A **361**, 1655–1674 (2003).
2. J. Yin, Y. Cao, Y.-H. Li, S.-K. Liao, L. Zhang, J.-G. Ren, W.-Q. Cai, W.-Y. Liu, B. Li, H. Dai, G.-B. Li, Q.-M. Lu, Y.-H. Gong, Y. Xu, S.-L. Li, F.-Z. Li, Y.-Y. Yin, Z.-Q. Jiang, M. Li, J.-J. Jia, G. Ren, D. He, Y.-L. Zhou, X.-X. Zhang, N. Wang, X. Chang, Z.-C. Zhu, N.-L. Liu, Y.-A. Chen, C.-Y. Lu, R. Shu, C.-Z. Peng, J.-Y. Wang, and J.-W. Pan, "Satellite-based entanglement distribution over 1200 kilometers," Science **356**, 1140–1144 (2017).
3. M. Kues, C. Reimer, P. Roztocki, L. R. Cortés, S. Sciara, B. Wetzel, Y. Zhang, A. Cino, S. T. Chu, B. E. Little, D. J. Moss, L. Caspani, J. Azaña, and R. Morandotti, "On-chip generation of high-dimensional entangled quantum states and their coherent control," Nature **546**, 622–626 (2017).
4. J. Wang, S. Paesani, Y. Ding, R. Santagati, P. Skrzypczyk, A. Salavrakos, J. Tura, R. Augusiak, L. Mančinska, D. Bacco, D. Bonneau, J. W. Silverstone, Q. Gong, A. Acín, K. Rottwitt, L. K. Oxenløwe, J. L. O'Brien, A. Laing, and M. G. Thompson, "Multidimensional quantum entanglement with large-scale integrated optics," Science **360**, 285–291 (2018).
5. M. Giustina, S. Versteegh, M. A. Wengerowsky, J. Handsteiner, A. Hochrainer, K. Phelan, F. Steinlechner, J. Kofler, J.-Å. Larsson, C. Abellán, W. Amaya, V. Pruneri, M. W. Mitchell, J. Beyer, T. Gerrits, A. E. Lita, L. K. Shalm, S. W. Nam, T. Scheidl, R. Ursin, B. Wittmann, and A. Zeilinger, "Significant-loophole-free test of Bell's theorem with entangled photons," Phys. Rev. Lett. **115**, 250401 (2015).
6. L. K. Shalm, E. Meyer-Scott, B. G. Christensen, P. Bierhorst, M. A. Wayne, M. J. Stevens, T. Gerrits, S. Glancy, D. R. Hamel, M. S. Allman, K. J. Coakley, S. D. Dyer, C. Hodge, A. E. Lita, V. B. Verma, C. Lambrocco, E. Tortorici, A. L. Migdall, Y. Zhang, D. R. Kumor, W. H. Farr, F. Marsili, M. D. Shaw, J. A. Stern, C. Abellán, W. Amaya, V. Pruneri, T. Jennewein, M. W. Mitchell, P. G. Kwiat, J. C. Bienfang, R. P. Mirin, E. Knill, and S. W. Nam, "Strong loophole-free test of local realism," Phys. Rev. Lett. **115**, 250402 (2015).
7. N. Gisin, G. Ribordy, W. Tittel, and H. Zbinden, "Quantum cryptography," Rev. Mod. Phys. **74**, 145–195 (2002).
8. F. Xu, X. M. Zhang, H.-K. Lo, and J.-W. Pan, "Quantum cryptography with realistic devices," arXiv:1903.09051 (2019).
9. N. J. Cerf, M. Bourennane, A. Karlsson, and N. Gisin, "Security of quantum key distribution using d-level systems," Phys. Rev. Lett. **88**, 127902 (2002).
10. H. Bechmann-Pasquinucci and W. Tittel, "Quantum cryptography using larger alphabets," Phys. Rev. A **61**, 062308 (2000).
11. S. Ecker, F. Bouchard, L. Bulla, F. Brandt, O. Kohout, F. Steinlechner, R. Fickler, M. Malik, Y. Guryanova, R. Ursin, and M. Huber, "Overcoming noise in entanglement distribution," Phys. Rev. X **9**, 041042 (2019).
12. J. Bavaresco, N. Herrera Valencia, C. Klöckl, M. Pivoluska, P. Erker, N. Friis, M. Malik, and M. Huber, "Measurements in two bases are sufficient for certifying high-dimensional entanglement," Nat. Phys. **14**, 1032–1037 (2018).
13. M. Erhard, R. Fickler, M. Krenn, and A. Zeilinger, "Twisted photons: new quantum perspectives in high dimensions," Light Sci. Appl. **7**, 17146 (2018).

14. H. Rubinsztein-Dunlop, A. Forbes, M. V. Berry, M. R. Dennis, D. L. Andrews, M. Mansuripur, C. Denz, C. Alpmann, P. Banzer, T. Bauer, E. Karimi, L. Marrucci, M. Padgett, M. Ritsch-Marte, N. M. Litchinitser, N. P. Bigelow, C. Rosales-Guzmán, A. Belmonte, J. P. Torres, T. W. Neely, M. Baker, R. Gordon, A. B. Stilgoe, J. Romero, A. G. White, R. Fickler, A. E. Willner, G. Xie, B. McMorran, and A. M. Weiner, "Roadmap on structured light," J. Opt. **19**, 013001 (2017).
15. L. Allen, M. W. Beijersbergen, R. J. C. Spreeuw, and J. P. Woerdman, "Orbital angular momentum of light and the transformation of Laguerre-Gaussian laser modes," Phys. Rev. A **45**, 8185–8189 (1992).
16. R. Fickler, G. Campbell, B. Buchler, P. K. Lam, and A. Zeilinger, "Quantum entanglement of angular momentum states with quantum numbers up to 10, 010," Proc. Natl. Acad. Sci. USA **113**, 13642–13647 (2016).
17. E. Karimi and E. Santamato, "Radial coherent and intelligent states of paraxial wave equation," Opt. Lett. **37**, 2484–2486 (2012).
18. E. Karimi, R. W. Boyd, P. De La Hoz, H. De Guise, J. Řeháček, Z. Hradil, A. Aiello, G. Leuchs, and L. L. Sánchez-Soto, "Radial quantum number of Laguerre-Gauss modes," Phys. Rev. A **89**, 063813 (2014).
19. E. Karimi, D. Giovannini, E. Bolduc, N. Bent, F. M. Miatto, M. J. Padgett, and R. W. Boyd, "Exploring the quantum nature of the radial degree of freedom of a photon via Hong-Ou-Mandel interference," Phys. Rev. A **89**, 013829 (2014).
20. W. N. Plick and M. Krenn, "Physical meaning of the radial index of Laguerre-Gauss beams," Phys. Rev. A **92**, 063841 (2015).
21. A. Mair, A. Vaziri, G. Weihs, and A. Zeilinger, "Entanglement of the orbital angular momentum states of photons," Nature **412**, 313–316 (2001).
22. M. Krenn, M. Huber, R. Fickler, R. Lapkiewicz, S. Ramelow, and A. Zeilinger, "Generation and confirmation of a (100 × 100)-dimensional entangled quantum system," Proc. Natl. Acad. Sci. USA **111**, 6243–6247 (2014).
23. M. Mirhosseini, O. S. Magaña-Loaiza, M. N. O'sullivan, B. Rodenburg, M. Malik, M. P. J. Lavery, M. J. Padgett, D. J. Gauthier, and R. W. Boyd, "High-dimensional quantum cryptography with twisted light," New J. Phys. **17**, 033033 (2015).
24. M. G. McLaren, F. S. Roux, and A. Forbes, "Realising high-dimensional quantum entanglement with orbital angular momentum," South African J. Sci. **111**, 1–9 (2015).
25. M. Malik, M. Erhard, M. Huber, M. Krenn, R. Fickler, and A. Zeilinger, "Multi-photon entanglement in high dimensions," Nat. Photonics **10**, 248–252 (2016).
26. A. Sit, F. Bouchard, R. Fickler, J. Gagnon-Bischoff, H. Larocque, K. Heshami, D. Elser, C. Peuntinger, K. Günthner, B. Heim, and C. Marquardt, "High-dimensional intracity quantum cryptography with structured photons," Optica **4**, 1006–1010 (2017).
27. F. Bouchard, R. Fickler, R. W. Boyd, and E. Karimi, "High-dimensional quantum cloning and applications to quantum hacking," Sci. Adv. **3**, e1601915 (2017).
28. F. Cardano, F. Massa, H. Qassim, E. Karimi, S. Slussarenko, D. Paparo, C. de Lisio, F. Sciarrino, E. Santamato, R. W. Boyd, and L. Marrucci, "Quantum walks and wavepacket dynamics on a lattice with twisted photons," Sci. Adv. **1**, e1500087 (2015).
29. F. Cardano, A. D'Errico, A. Dauphin, M. Maffei, B. Piccirillo, C. de Lisio, G. De Filippis, V. Cataudella, E. Santamato, L. Marrucci, M. Lewenstein, and P. Massignan, "Detection of Zak phases and topological invariants in a chiral quantum walk of twisted photons," Nat. Commun. **8**, 15516 (2017).
30. N. R. Heckenberg, R. McDuff, C. P. Smith, and A. G. White, "Generation of optical phase singularities by computer-generated holograms," Opt. Lett. **17**, 221–223 (1992).
31. A. Forbes, A. Dudley, and M. McLaren, "Creation and detection of optical modes with spatial light modulators," Adv. Opt. Photon. **8**, 200–227 (2016).
32. G. Turnbull, D. Robertson, G. Smith, L. Allen, and M. Padgett, "The generation of free-space Laguerre-Gaussian modes at millimetre-wave frequencies by use of a spiral phaseplate," Opt. Commun. **127**, 183–188 (1996).
33. L. Marrucci, C. Manzo, and D. Paparo, "Optical spin-to-orbital angular momentum conversion in inhomogeneous anisotropic media," Phys. Rev. Lett. **96**, 163905 (2006).
34. G. C. G. Berkhout, M. P. J. Lavery, J. Courtial, M. W. Beijersbergen, and M. J. Padgett, "Efficient sorting of orbital angular momentum states of light," Phys. Rev. Lett. **105**, 153601 (2010).
35. M. Mirhosseini, M. Malik, Z. Shi, and R. W. Boyd, "Efficient separation of the orbital angular momentum eigenstates of light," Nat. Commun. **4**, 2781 (2013).
36. J. Leach, M. J. Padgett, S. M. Barnett, S. Franke-Arnold, and J. Courtial, "Measuring the orbital angular momentum of a single photon," Phys. Rev. Lett. **88**, 257901 (2002).
37. M. N. O'sullivan, M. Mirhosseini, M. Malik, and R. W. Boyd, "Near-perfect sorting of orbital angular momentum and angular position states of light," Opt. Express **20**, 24444–24449 (2012).
38. Y. Zhou, M. Mirhosseini, D. Fu, J. Zhao, S. M. Hashemi Rafsanjani, A. E. Willner, and R. W. Boyd, "Sorting photons by radial quantum number," Phys. Rev. Lett. **119**, 263602 (2017).
39. N. K. Fontaine, R. Ryf, H. Chen, D. T. Neilson, K. Kim, and J. Carpenter, "Laguerre-Gaussian mode sorter," Nat. Commun. **10**, 1865 (2019).
40. N. K. Fontaine, R. Ryf, H. Chen, D. Neilson, and J. Carpenter, "Design of high order mode-multiplexers using multiplane light conversion," in *European Conference on Optical Communication (ECOC)* (IEEE, 2017), pp. 1–3.
41. X. Gu, M. Krenn, M. Erhard, and A. Zeilinger, "Gouy phase radial mode sorter for light: concepts and experiments," Phys. Rev. Lett. **120**, 103601 (2018).
42. R. Fickler, F. Bouchard, E. Giese, V. Grillo, G. Leuchs, and E. Karimi, "Full-field mode sorter using two optimized phase transformations for high-dimensional quantum cryptography,"J. Opt. **22**, 024001 (2020).
43. F. Bouchard, N. H. Valencia, F. Brandt, R. Fickler, M. Huber, and M. Malik, "Measuring azimuthal and radial modes of photons," Opt. Express **26**, 31925–31941 (2018).
44. J. Courtial and M. Padgett, "Performance of a cylindrical lens mode converter for producing Laguerre-Gaussian laser modes," Opt. Commun. **159**, 13–18 (1999).
45. S. Slussarenko, E. Karimi, B. Piccirillo, L. Marrucci, and E. Santamato, "Universal unitary gate for single-photon spin-orbit four-dimensional states," Phys. Rev. A **80**, 022326 (2009).
46. F. Schlederer, M. Krenn, R. Fickler, M. Malik, and A. Zeilinger, "Cyclic transformation of orbital angular momentum modes," New J. Phys. **18**, 043019 (2016).
47. A. Babazadeh, M. Erhard, F. Wang, M. Malik, R. Nouroozi, M. Krenn, and A. Zeilinger, "High-dimensional single-photon quantum gates: concepts and experiments," Phys. Rev. Lett. **119**, 180510 (2017).
48. X. Gao, M. Krenn, J. Kysela, and A. Zeilinger, "Arbitrary d -dimensional Pauli X gates of a flying qudit," Phys. Rev. A **99**, 023825 (2019).
49. C. Schaeff, R. Polster, M. Huber, S. Ramelow, and A. Zeilinger, "Experimental access to higher-dimensional entangled quantum systems using integrated optics," Optica **2**, 523–529 (2015).
50. P. Imany, J. A. Jaramillo-Villegas, M. S. Alshaykh, J. M. Lukens, O. D. Odele, A. J. Moore, D. E. Leaird, M. Qi, and A. M. Weiner, "High-dimensional optical quantum logic in large operational spaces," Quantum Inf. **5**, 1–10 (2019).
51. J.-F. Morizur, L. Nicholls, P. Jian, S. Armstrong, N. Treps, B. Hage, M. Hsu, W. Bowen, J. Janousek, and H.-A. Bachor, "Programmable unitary spatial mode manipulation," J. Opt. Soc. Am. A **27**, 2524–2531 (2010).
52. G. Labroille, B. Denolle, P. Jian, P. Genevaux, N. Treps, and J.-F. Morizur, "Efficient and mode selective spatial mode multiplexer based on multi-plane light conversion," Opt. Express **22**, 15599–15607 (2014).
53. H. Takahashi, T. Saida, T. Hashimoto, and Y. Sakamaki, "New optical waveguide design based on wavefront matching method," J. Lightwave Technol. **25**, 3511–3518 (2007).
54. S. Bade, B. Denolle, G. Trunet, N. Riguet, P. Jian, O. Pinel, and G. Labroille, "Fabrication and characterization of a mode-selective 45-mode spatial multiplexer based on multi-plane light conversion," in *Proceedings of the Optical Fiber Communications Conference and Exposition (OFC)* (Institute of Electrical and Electronics Engineers Inc., 2018), pp. 1–3.
55. P. Boucher, N. Barré, O. Pinel, G. Labroille, and N. Treps, "Continuous axial scanning of a Gaussian beam via beam steering," Opt. Express **25**, 23060–23069 (2017).
56. V. Scarani, H. Bechmann-Pasquinucci, N. J. Cerf, M. Dušek, N. Lütkenhaus, and M. Peev, "The security of practical quantum key distribution," Rev. Mod. Phys. **81**, 1301–1350 (2009).
57. F. Bouchard, F. Hufnagel, D. Koutný, A. Abbas, A. Sit, K. Heshami, R. Fickler, and E. Karimi, "Quantum process tomography of a high-dimensional quantum communication channel," Quantum **3**, 138 (2019).

58. S. Rahimi-Keshari, M. A. Broome, R. Fickler, A. Fedrizzi, T. C. Ralph, and A. G. White, "Direct characterization of linear-optical networks," Opt. Express **21**, 13450–13458 (2013).
59. A. Gilchrist, N. K. Langford, and M. A. Nielsen, "Distance measures to compare real and ideal quantum processes," Phys. Rev. A **71**, 062310 (2005).
60. E. Bolduc, N. Bent, E. Santamato, E. Karimi, and R. W. Boyd, "Exact solution to simultaneous intensity and phase encryption with a single phase-only hologram," Opt. Lett. **38**, 3546–3549 (2013).
61. R. L. Haupt and S. Ellen Haupt, *Practical Genetic Algorithms* (Wiley Online Library, 2004).
62. B. P. Lanyon, M. Barbieri, M. P. Almeida, T. Jennewein, T. C. Ralph, K. J. Resch, G. J. Pryde, J. L. O'brien, A. Gilchrist, and A. G. White, "Simplifying quantum logic using higher-dimensional Hilbert spaces," Nat. Phys. **5**, 134–140 (2009).